European Journal of Medicinal Chemistry 76 (2014) 397–407

Contents lists available at ScienceDirect

European Journal of Medicinal Chemistry

journal homepage: http://www.elsevier.com/locate/ejmech

Original article

Copper complexes with phosphonium containing hydrazone ligand: Topoisomerase inhibition and cytotoxicity study

Shin Thung Chew [a], Kong Mun Lo [a,*], Sze Koon Lee [a], Mok Piew Heng [a], Wuen Yew Teoh [b], Kae Shin Sim [b], Kong Wai Tan [a,*]

[a] Department of Chemistry, Faculty of Science, University of Malaya, 50603 Kuala Lumpur, Malaysia
[b] Institute of Biological Sciences, Faculty of Science, University of Malaya, 50603 Kuala Lumpur, Malaysia

ARTICLE INFO

Article history:
Received 11 October 2013
Received in revised form
17 February 2014
Accepted 18 February 2014
Available online 19 February 2014

Keywords:
Hydrazones
Cytotoxicity
Topoisomerase I inhibitor
Copper(II) complexes

ABSTRACT

Four new copper(II) complexes containing phosphonium substituted hydrazone (L) with the formulations [CuL]Cl(**3**), [Cu(phen)L]Cl(**4**), [Cu(bpy)L]Cl(**5**), [Cu(dbpy)L]Cl(**6**), (where L = doubly deprotonated hydrazone; phen = 1,10′-phenanthroline; bpy = 2,2′-bipyridine; dbpy = 5,5′-dimethyl-2,2′-bipyridine) have been synthesized. The compounds were characterized by elemental analysis, spectroscopic methods and in the case of crystalline products by X-ray crystallography. The cytotoxicity and topoisomerase I (topo I) inhibition activities of these compounds were studied. It is noteworthy that the addition of N,N-ligands to the copper(II) complex lead to the enhancement in the cytotoxicity of the compounds, especially against human prostate adenocarcinoma cell line (PC-3). Complex **4** exhibits the highest activity against PC-3 with the IC_{50} value of 3.2 μM. The complexes can also inhibit topo I through the binding to DNA and the enzyme.

1. Introduction

Success of cisplatin as an anticancer agent has drawn the attention of many chemists towards the development of new metal based drugs in order to overcome the drawbacks of cisplatin [1–4]. Copper is well known as a bio-essential element for human and its complexes have proved to be excellent for biological applications which include the treatment of cancers [5–8]. Over the last decade, Schiff bases are gaining prominence in medicinal chemistry due to its great chemotherapeutic application [9,10]. It is believed that the type of coordinated ligands and the geometrical orientation of the ligands are crucial factors in promoting the interaction of a given metal complex with DNA.

Recently, Krishnamoorthy and co-workers have shown that copper hydrazones complexes have better potential than other metal complexes in the conversion of DNA from supercoiled form (form I) to the nicked circular form (form II) [11]. Apart from that, there are also numerous copper complexes of hydrazone which possess anticancer properties [12–18]. Therefore, copper hydrazones complexes are one of the important candidates in metal based drugs research. On the other hand, heterocyclic bases play a pivotal role in many biological application and significantly enhanced interaction with DNA [19,20]. Cytotoxic activities of several copper(II) complexes have already been evaluated for their potential antitumour activities on different cell lines [21,22]. Topoisomerases have been identified as important targets in cancer chemotherapy and are among the most widely clinically used anticancer drugs [23–25]. Yet, very few metal complexes have been reported to inhibit topoisomerases in contrast to organic molecules [26,27]. Based on the above findings, we attempt to develop a new series of copper(II) complexes containing 5-(triphenylphosphoniummethyl)-salicylaldehyde benzoylhydrazone] chloride ligand (**2**) and heterocyclic bases such as 1,10′-phenanthroline (phen), 2,2′-bipyridine (bpy) and 5,5′-dimethyl-2,2′-bipyridine (dbpy) as copper based anticancer agents. In order to gain better insight into the mode of action of these potentially cytotoxic compounds, we report herein the first example for the interaction of copper complexes of hydrazone ligand with topoisomerase I.

2. Results and discussion

2.1. Syntheses and characterization

The reaction scheme for the synthesis of copper complexes was presented in Scheme 1. The complexes were highly soluble in DMSO, DMF and methanol. They are non-hygroscopic and stable both in solid and solution phases. The elemental analyses data for

* Corresponding authors.

http://dx.doi.org/10.1016/j.ejmech.2014.02.049
0223-5234/

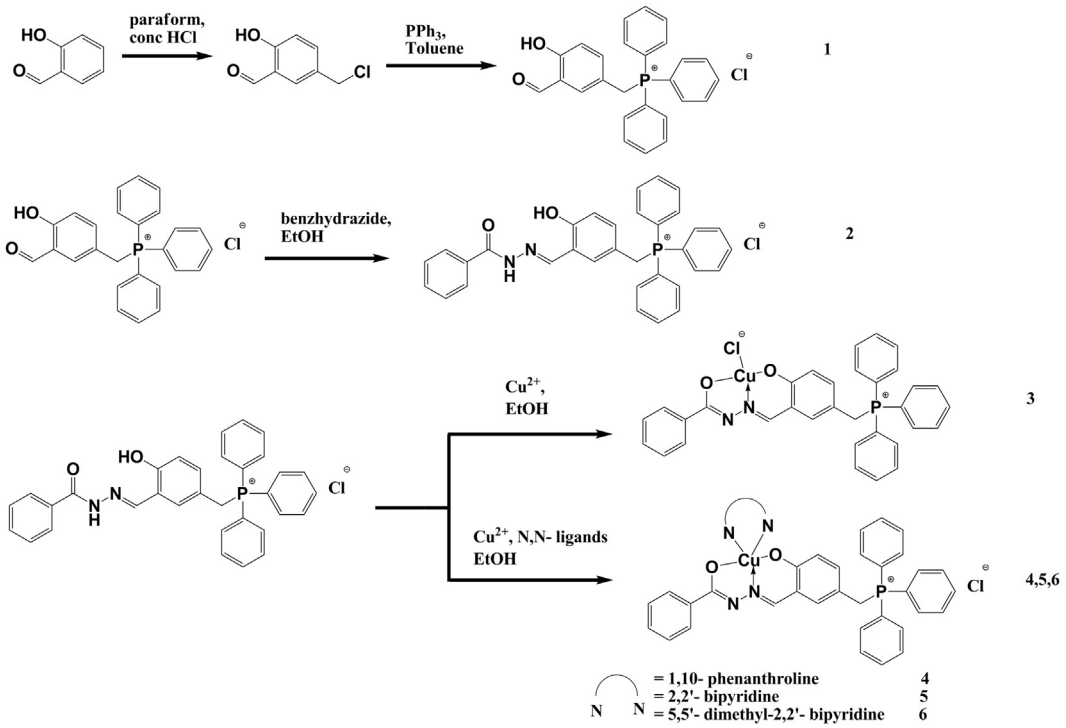

Scheme 1. Reaction scheme and proposed structures.

the Cu(II) complexes are in good agreement with the molecular formulae of the complexes. Compound **1** is white in colour while Schiff base ligand **2** is yellow and all the metal complexes are green.

2.2. Infrared spectra

The IR spectra of the complexes in the region 4000–400 cm^{-1} were analyzed. In comparison with the free ligand, the data gave evidence of coordination of ligand **2** to the copper metal ion *via* phenolate oxygen, azomethine nitrogen and enolate oxygen. In the IR spectrum of **2**, a strong band at 1679 cm^{-1} has disappeared in all the IR spectra of complexes which is assigned to the stretching vibration of carbonyl [ν(C=O)] [19,28]. The infrared spectra of **3**–**6** display IR absorption bands at 1613, 1612, 1612, and 1612 cm^{-1} respectively which are ascribed to the ν(C=N) stretching frequencies of the complexes, whereas for the free ligand the same band was observed at 1619 cm^{-1}. The shift of this band on complexation towards lower wavenumbers indicates the coordination of azomethine nitrogen ν(C=N) to the copper centre [11,18,29]. The appearance of the bands in the 1500–1503 cm^{-1} range in the complexes are due to the asymmetric stretching vibration of the newly formed N=C bond as a result of the enolization of ligand (**2**) [11,30]. In addition, the characteristic ν(N–N) stretching of the free ligand **2** (observed at 1028 cm^{-1}) undergoes a positive shift to a higher wavenumber upon complexation which is attributed to the diminished repulsion between the lone pairs of adjacent nitrogen atoms [31–33]. The formation of complexes **3**–**6** have been confirmed by the presence of bands around ~489 and ~517 cm^{-1} corresponding to ν(Cu–N) and ν(Cu–O) respectively [19,28,30].

2.3. Electronic spectra

The significant electronic absorption bands in the spectra of the ligand **2** and all the complexes recorded in methanol solution are presented in Table 1 and the spectra are shown in Figs. S1 and S2. The bands in the region of 312–328 nm and 228–276 nm of complexes **3**–**6** are due to the $n \rightarrow \pi^*$ and $\pi \rightarrow \pi^*$ transitions of the hydrazone ligands and the coordinated diimine ligands [19,29]. The $n \rightarrow \pi^*$ transition, which appears in the region of 289–300 nm in the spectrum of the uncomplexed hydrazone ligand was slightly shifted to a higher wavelength upon complexation. This is an indication of the enolization followed by the deprotonation of the ligand during complexation [30]. The broad bands observed at approximately 400 nm are attributed to the ligand-to-metal-charge transfer (LMCT) transition [11,29,33]. Their broadness may be due to the overlapping of the LMCT transitions of O → Cu and N → Cu. The complexes with N,N donor ligands (**4**–**6**) displayed d–d bands in the 649–655 nm range, which tend to be indicative of a distorted square pyramidal geometry [19] while complex **3** that displays a square planar coordination, absorbs at 636 nm [34].

2.4. ^1H- and ^{13}C- NMR

Additional structural information can be deduced from the ^1H NMR and ^{13}C NMR spectra and relevant chemical shifts are presented in Tables S1 and S2. Since copper(II) complexes are paramagnetic in nature, its NMR spectrum could not be obtained. In the ^1H NMR spectrum of compound **1**, the chemical shift for the aldehydic proton appears at 10.10 ppm. Upon the formation of Schiff base ligand **2**, the aldehydic proton (–CHO) is replaced by azomethine proton (N=CH) which is shifted upfield to 8.46 ppm. The formation of ligand **2** is further corroborated by the presence of –NH proton at 12.24 ppm. The multiplets that appear at the region of 7.62–7.89 ppm are ascribed to the aromatic protons from triphenylphosphine, whereas the aromatic protons of the benzhydrazide appear in the region of 7.49–7.59 ppm and 7.91–7.93 ppm. The sharp doublets signal around 5.00 ppm is assigned to the methylene proton.

Table 1
Electronic spectral assignments, λ/nm (ε/Lcm^{-1} mol^{-1}) for ligand and its copper(II) complexes in methanol.

Compounds	d–d	LMCT	$n \rightarrow \pi^*$	$\pi \rightarrow \pi^*$
2	–	–	289 (54,521.6), 300 (51,044.8)	277 (51,250.4)
3	636 (158.57)	392 (34,970.4)	313 (39,570.4), 328 (36,924.0)	228 (92,246.4), 269 (55,742.4)
4	655 (165.16)	391 (34,043.2)	312 (43,261.6), 327 (37383.2)	228 (153,222.4), 268 (103,222.4)
5	649 (162.23)	392 (35,322.4)	312 (41,484.0), 328 (37,324.0)	229 (111,669.6), 276 (76,757.6)
6	655 (161.01)	392 (34,365.6)	312 (48,252), 327 (37,284.8)	229 (106,865.6), 270 (71,025.6)

From ^{13}C NMR spectrum of compound **1**, the chemical shift at 189.41 ppm and 160.83 ppm is due to C=O and C–OH respectively. It is noteworthy that when compound **1** condensed with benzhydrazide, the chemical shift of carbonyl carbon (C=O) is replaced by azomethine carbon (C=N) in ligand **2** with 146.80 ppm. Additionally, the signal at 162.95 ppm is ascribed to the carbonyl carbon from the benzhydrazide. The doublet that falls around 27.00 ppm is assigned to the methylene carbon for both **1** and **2**.

2.5. X-ray crystal structures

Compounds **1**–**5** were structurally characterized by single crystal X-ray crystallography. Selected crystallographic data are summarized in Table 2. Figs. 1–5 show the ORTEP plots of compounds **1**–**5**. Selected bond lengths and angles are given in Table 3. The chloromethylation of salicylaldehyde followed by the addition of triphenylphosphine yielded (3-formyl-4-hydroxybenzyl)triphenylphosphonium chloride (**1**). Its asymmetric unit (Fig. 1) consists of two crystallographically independent cations and two chloride counterions linked to the cations *via* an O–H···Cl hydrogen bonding interaction [O1–H1···Cl2 = 2.983(2) Å, symmetry operator: $-x, -y + 1, -z$; O3–H3···Cl1 = 2.996(2) Å, symmetry operator: $-x, -y + 1, -z$] (Table 4). The condensation of **1** with benzhydrazide gave the Schiff base ligand, [5-(triphenylphosphoniummethyl)-salicylaldehyde benzohydrazone] chloride monohydrate (**2**). The unit cell of compound **2** as depicted in Fig. 2 also consists of two molecules which are linked together by hydrogen bonding between the water molecule and imino hydrogen with the chloride anion. In addition, the presence of intramolecular hydrogen bonding between the phenolate hydroxyl group and the azomethine nitrogen stabilizes the molecules. The relatively short bond distances of C60–O4 [1.223(3) Å] and C27–O2 [1.222(3) Å] compared to those of C56–O3 [1.356(3) Å] and C23–O1 [1.354(3) Å] (Table 3) indicate that the Schiff base exists predominantly in keto configuration in the solid phase.

As can be seen from Fig. 3, the copper ion is coordinated to the tridentate hydrazone ligand, through the phenolate oxygen (O1), azomethine nitrogen (N1) and enolate oxygen (O2) and with a

Table 2
Crystallographic data for compounds **1**–**5**.

Compounds	**1**	**2**	**3**	**4**	**5**
Chemical formula	$C_{26}H_{22}ClO_2P$	$C_{33}H_{30}ClN_2O_3P$	$C_{33}H_{26}ClCuN_2O_{2.38}P$	$C_{47}H_{42}ClCuN_4O_4P$	$C_{45}H_{42}ClCuN_5O_4P$
M_r	432.86	569.01	618.52	856.81	846.80
Crystal system	Triclinic, *P*-1	Triclinic, *P*-1	Monoclinic, *P*2 (1)/*c*	Triclinic, *P*-1	Triclinic, *P*-1
Unit cell dimension					
a (Å)	9.7734 (1)	10.2722 (2)	8.6309 (3)	10.4487 (2)	12.3972 (2)
b (Å)	13.0679 (2)	16.1112 (3)	23.3370 (8)	13.5982 (5)	12.9623 (2)
c (Å)	17.6675 (2)	19.5664 (4)	14.3886 (5)	15.4688 (5)	14.3509 (2)
α (°)	105.527 (1)	68.629 (1)		110.199 (3)	97.526 (1)
β (°)	92.536 (1)	78.208 (1)	106.307 (2)	100.089 (2)	112.581 (1)
γ (°)	90.629 (1)	73.093 (1)		90.576 (2)	104.634 (1)
V (Å^3)	2171.36 (5)	2867.6 (1)	2781.6 (2)	2024.9 (1)	1992.05 (5)
Z	4	4	4	2	2
F (000)	904	1192	1272	890	880
Dx (Mg m^{-3})	1.324	1.318	1.477	1.405	1.412
θ (°)	2.4–28.3	2.5–26.9	2.6–23.5	2.5–29.3	2.6–28.4
μ (mm^{-1})	0.27	0.23	0.98	0.70	0.71
T (*K*)	100 (2)	100 (2)	100 (2)	100 (2)	100 (2)
Crystal colour, habit	Colourless, Block	Yellow, Block	Green, Block	Green, Block	Green, Block
Crystal size (mm)	0.10 × 0.05 × 0.04	0.10 × 0.10 × 0.05	0.20 × 0.15 × 0.08	0.20 × 0.05 × 0.02	0.1 × 0.08 × 0.05
T_{min}	0.974	0.978	0.829	0.873	0.649
T_{max}	0.989	0.989	0.926	0.986	0.746
Observed data [$I > 2\sigma(I)$]	7215	7573	3711	6328	8202
R_{int}	0.029	0.042	0.071	0.022	0.016
θ_{max} (°)	26.5	25.5	25.5	25.0	27.5
θ_{min} (°)	1.2	1.1	2.3	2.5	1.9
h	−12 to 12	−12 to 12	−10 to 10	−12 to 12	−16 to 16
k	−16 to 16	−19 to 19	−28 to 26	−16 to 11	−16 to 16
l	−22 to 22	−23 to 23	−17 to 17	−17 to 18	−18 to 18
R [$F^2 > 2\sigma(F^2)$]	0.040	0.046	0.047	0.036	0.035
wR (F^2)	0.104	0.121	0.123	0.099	0.102
S	1.05	1.02	1.02	1.07	1.04
$\Delta\rho_{max}$ (e Å^{-3})	0.45	0.40	0.96	0.70	0.67
$\Delta\rho_{min}$ (e Å^{-3})	−0.31	−0.30	−0.51	−0.57	−0.30
CCDC number	957,702	957,703	957,704	957,705	957,706

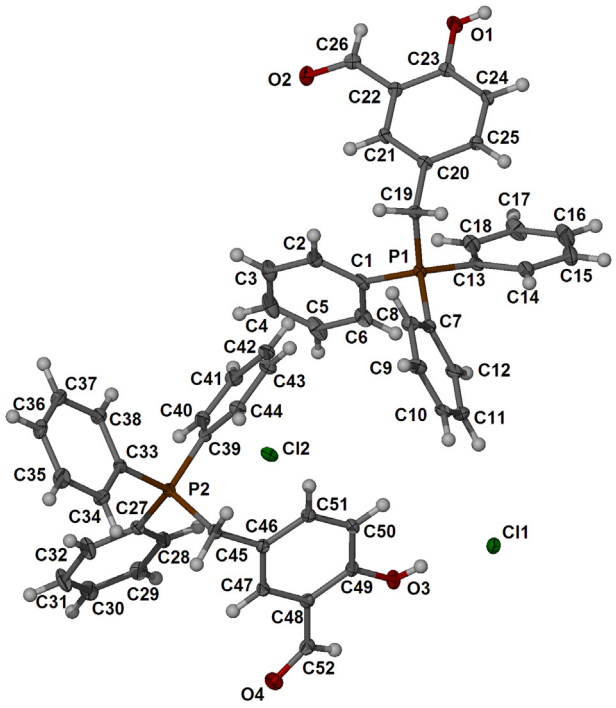

Fig. 1. An ORTEP view of **1** showing the atom labelling scheme (50% probability thermal ellipsoids).

fourth bond formed between the copper metal and a chloride ion. This gives rise to a zwitterion species with a positive charge at the phosphorus centre. The transoid angles N1–Cu1–Cl1 [174.63(9)°] and O1–Cu1–O2 [172.8(1)°] which deviate from the values of 180° [34] and the sum (Σ) of the six inter-bond angles for complex **3** is 707°, which deviates from the ideal angle of 720°, suggesting that the copper centre adopts a distorted square planar geometry [35,36]. Further evidence can be seen from the small dihedral angle of 4.6(1)° formed between the two near planar rings Cu1–N1–N2–C24–O2 (RMS deviation = 0.0013 Å) and Cu1–N1–C31–C32–C23–O1 rings (RMS deviation = 0.0065 Å). The relative small difference between the bond distances of C23–O1 [1.317(4) Å] and C24–O2 [1.295(4) Å] shows that the Schiff base adopts the enol configuration when coordinated to the copper ion. There is a water molecule (O3) that persists in the molecular structure which was found to be disordered and was refined with a chemical occupancy of 0.38.

On the other hand, the reaction of copper(II) ion with hydrazone ligand **2** in the presence of 1,10′-phenanthroline and ethanol afforded the copper complex **4** (Fig. 4) and **5** (Fig. 5), which has a five coordinated copper centre, with a distorted square pyramidal bonding pattern. The basal plane of the distorted square pyramidal coordination is formed by the dianionic tridentate ONO-donor ligand and the N4 atom of phen, while the axial position is occupied by N3 of phen. One of the reasons for the deviation from an ideal stereochemistry is the restricted bite angle imposed both by the ONO-donor hydrazone ligand [O1–Cu1–N1 = 92.67(7)°, N1–Cu1–O2 = 81.23(7)°] and the phen ligand [N3–Cu1–N4 = 78.84(8)°] [30]. As with complex **3**, the small differences between the bond distances of C23–O1 [1.315(3) Å] and C24–O2 [1.288(3) Å] and those of Cu1–O1 [1.919(2) Å] and Cu1–O2 [1.946(2) Å] also indicate that the copper(II) ion is coordinated to the enolized form of the Schiff base ligand. The presence of an ethanol and a water molecule links the chloride ion to the cationic copper complex *via* the H-bonding interactions with the enolate oxygen of the ligand [O3–H3A···Cl1 = 3.097(2), O4–H4A···O1 = 2.833(3) Å].

In complex **5**, the Schiff base is situated on the basal plane and bpy displays axial (N3)-equatorial (N4) coordination. Furthermore, it is solvated by an acetonitrile and two water molecules in which the hydrogen atoms of the water molecules are H bond donors to the chloride ion and the enolate oxygen atoms of an inversion related molecule, forming a dimeric unit in its crystal packing. In addition, there is an appreciable pseudo Jahn-Teller effect highlighted by Cu1–N3 distance [2.237(2) Å] which is significantly longer than that observed for the equatorial Cu1–N4 distance [2.018(2) Å] [37]. It has long been proven that Jahn-Teller effect is operative in the case of d^9 transition metal complexes. Thus, one trans pair of coordination bonds are elongated while the remaining four are shortened [11]. Akin to complex **4**, the angle formed between copper metal center and diimine ligand bpy [77.55(6) o] is known to be a standard bite angle [19,29]. The trigonality index, τ is calculated using the equation $\tau = (\beta - \alpha)/60$ [38] (for perfect square pyramidal and trigonal bipyramidal geometries the values of τ are zero and unity, respectively) [16,30,39]. The value of τ for **4** and **5** are 0.20 and 0.27 respectively which further affirm the geometry of distorted square pyramidal [38].

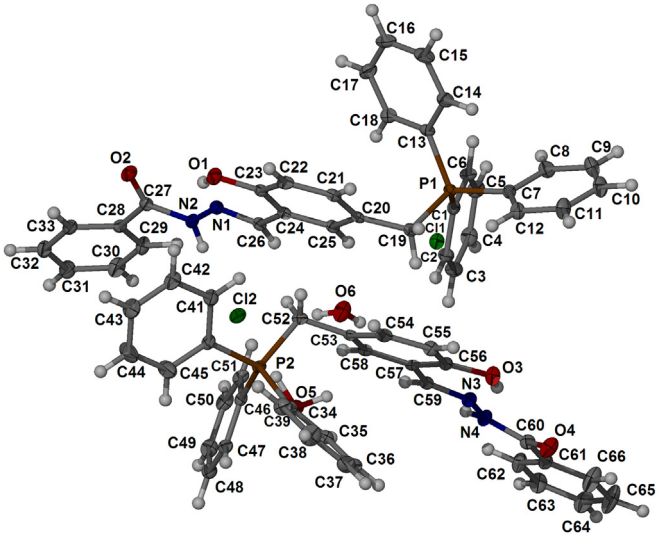

Fig. 2. An ORTEP view of **2** showing the atom labelling scheme (50% probability thermal ellipsoids).

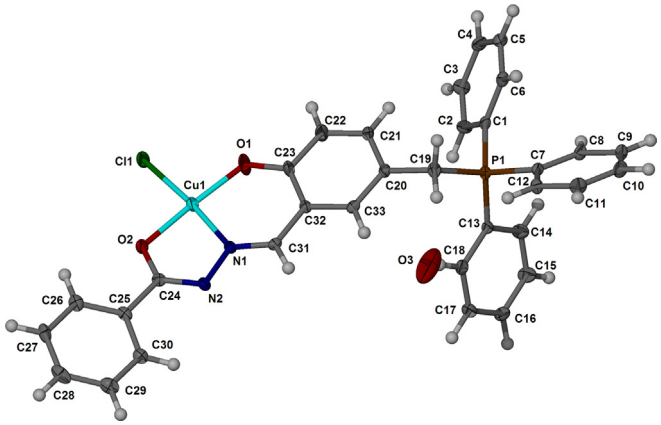

Fig. 3. An ORTEP view of **3** showing the atom labelling scheme (50% probability thermal ellipsoids).

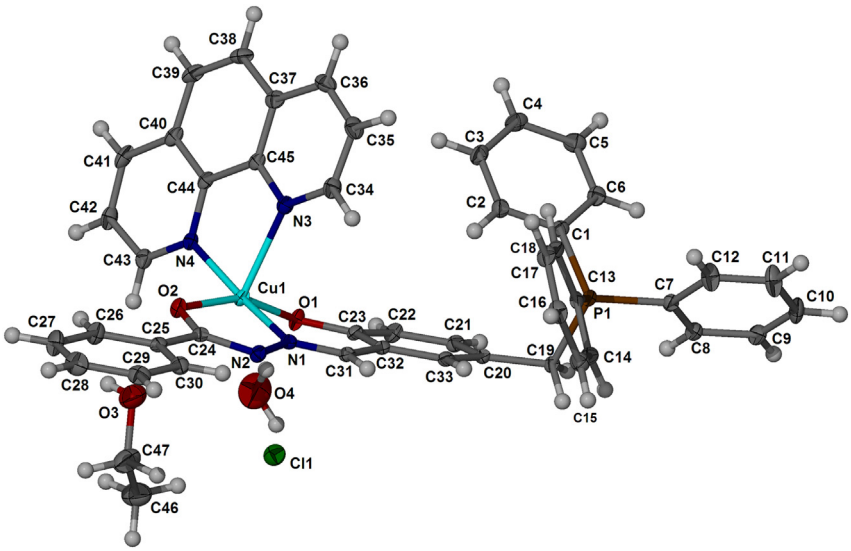

Fig. 4. An ORTEP view of **4** showing the atom labelling scheme (50% probability thermal ellipsoids).

3.6. Cytotoxic activity

Toxicity is a common limitation in terms of the introduction of new compounds into the pharmaceutical industry. In order to determine the *in vitro* cytotoxic activities of the compounds, experiments were carried out using human lung carcinoma cell line (A549), human prostate adenocarcinoma cell line (PC-3) and non-cancer human fibroblast cell line (MRC-5). Cell viability was determined by MTT assay after 72 h of treatment with increasing concentration of the compounds. The compounds were dissolved in DMSO and blanks samples containing same concentration of DMSO were taken as controls to identify the activity of solvents in this MTT assay. The results were analyzed by mean of cell viability expressed as IC_{50} values are shown in Table 5. Compound **1** is found to be less cytotoxic ($IC_{50} > 30$ μM) to cancerous and normal cells. It becomes cytotoxic when it is in the form of Schiff base ligand **2**. Surprisingly, complex **3** ($IC_{50} = 16.6 \pm 3.1$ μM) possess similar cytotoxicity with ligand **2** ($IC_{50} = 14.4 \pm 2.6$ μM) against PC-3 cell line. However, the addition of N, N ligands to the copper complex leads to an increase in cytotoxicity of compounds **4**–**6** with the lowest IC_{50} value of 3.2 μM for compound **4**. The cytotoxicity of the ternary complexes (**4**–**6**) decreases by the following order: **4** > **6** > **5**. The observed order of decrease reflects the important role of extended aromatic ring and hydrophobicity of the diimines in improving cytotoxicity.

In order to determine the selectivity of the compounds, the cytotocities of the compounds were tested on MRC-5 non-cancerous cell line. It is notably that complex **3** is non toxic, whereas ligand **2** is toxic towards normal cell line. Therefore, complexation of ligand **2** by copper leads to an enhancement in cytoselectivity. By comparing both tumour cell lines, all the compounds seems to be more toxic against PC-3 cell line than A549 cell line. Researchers point out that there is an increase of 2- to 10-fold of topo I enzyme in prostate tumours, compared to benign hyperplastic prostate tissue from the same patients [40]. Therefore, prostate carcinoma cells are good models to study compounds that are designed to target topo I. Complex **4** and **5** possess similar selectivity towards PC-3 cell line with the selectivity index (SI) of 1.59 and 1.58 respectively. Complexes bearing phen and bpy co-ligands are more selective towards cancerous cells were reported

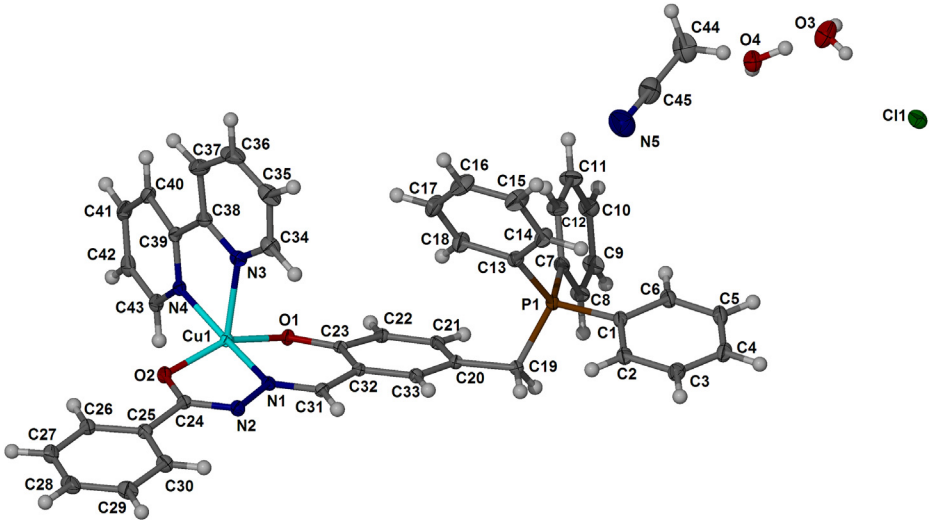

Fig. 5. An ORTEP view of **5** showing the atom labelling scheme (50% probability thermal ellipsoids).

Table 3
Selected bond lengths (Å) and bond angles (°) for compounds **1**–**5**.

Compound **1**			
O1–C23	1.346 (2)		
O2–C26	1.218 (3)		
O3–C49	1.349 (2)		
O4–C52	1.217 (3)		
Compound **2**			
N1–C26	1.290 (3)		
N1–N2	1.374 (3)		
N2–C27	1.372 (3)		
N3–C59	1.282 (3)		
N3–N4	1.369 (3)		
N4–C60	1.366 (3)		
O1–C23	1.354 (3)		
O2–C27	1.222 (3)		
O3–C56	1.356 (3)		
O4–C60	1.223 (3)		
Compound **3**			
Cl1–Cu1	2.229 (1)	O1–Cu1–N1	92.7 (1)
Cu1–O1	1.883 (3)	N1–Cu1–O2	81.3 (1)
Cu1–N1	1.930 (3)	O1–Cu1–Cl1	92.60 (9)
Cu1–O2	1.936 (3)	O2–Cu1–Cl1	93.46 (8)
N1–C31	1.287 (5)	N1–Cu1–Cl1	174.6 (1)
N1–N2	1.404 (4)	O1–Cu1–O2	172.8 (1)
N2–C24	1.314 (5)		
O1–C23	1.316 (5)		
O2–C24	1.295 (4)		
Compound **4**			
Cu1–O1	1.919 (2)	O1–Cu1–N1	92.67 (7)
Cu1–N1	1.926 (2)	N1–Cu1–O2	81.21 (7)
Cu1–O2	1.946 (2)	O1–Cu1–N4	95.07 (7)
Cu1–N4	2.003 (2)	O2–Cu1–N4	93.57 (7)
Cu1–N3	2.270 (2)	O1–Cu1–N3	96.72 (7)
N1–C31	1.293 (3)	N1–Cu1–N3	94.56 (7)
N1–N2	1.397 (3)	O2–Cu1–N3	104.70 (7)
N2–C24	1.329 (3)	N4–Cu1–N3	78.84 (8)
O1–C23	1.315 (3)		
O2–C24	1.288 (3)		
Compound **5**			
Cu1–N1	1.921 (2)	N1–Cu1–O1	92.64 (6)
Cu1–O1	1.948 (1)	N1–Cu1–O2	80.98 (6)
Cu1–O2	1.976 (1)	O1–Cu1–N4	92.85 (5)
Cu1–N4	2.018 (2)	O2–Cu1–N4	96.22 (6)
Cu1–N3	2.237 (2)	N1–Cu1–N3	95.82 (6)
N1–C31	1.289 (2)	O1–Cu1–N3	100.49 (5)
N1–N2	1.391 (2)	O2–Cu1–N3	103.54 (6)
N2–C24	1.321 (2)	N4–Cu1–N3	77.55 (6)
O1–C23	1.320 (2)		
O2–C24	1.293 (2)		

earlier [41–44]. Complex **6** is somehow lower in terms of selectivity with SI of 1.07. Delocalized lipophilic cations (DLC) are known to selectively accumulate in mitochondria of cancerous cells. Therefore, complexes with lipophilic cation moiety are known to be more sensitive towards cancer cells [45]. A general elevation in the mitochondrial membrane potential ($\Delta\Psi m$) has been linked to malignant transformation [46]. Compounds having lipophilic cation such as triphenylphosphonium moieties have been shown to dissipate the mitochondrial membrane potential upon uptake into mitochondria and lead to cell death [47,48]. This could be one of the possible explanations of better cytoselectivity of complex **4** and **5**. However, we have yet to come out with a plausible explanation for the lack of selectivity of complex **6** with a lipophilic cation moiety.

2.7. Topoisomerase I inhibition

DNA topoisomerase I (Topo I), an essential enzyme in metazoans has been identified as a target among the most widely used clinical drugs for treatment of cancer [49–51]. Topoisomerases have pivotal roles in DNA replication and transcription [28,40]. The enzymatic activity of topo I, like that of other topoisomerases, breaks the DNA backbone reversibly by replacing a DNA phosphodiester bond with a bond between a phosphate at one end of the DNA break and a tyrosine residue of the topo I protein [40,52–54]. In the case of topo I, the tyrosine links to the phosphate at the 3′-hydroxyl end of the DNA break. DNA relaxation takes place by rotation of the free end of the broken DNA around the intact DNA strand [55].

As a preliminary investigation of the topo I inhibition, we report herein the study by DNA relaxation assay. This assay provides a direct means of determination whether the drugs affect the unwinding of a supercoiled duplex DNA to a nicked open circular and relaxed DNA [28]. One unit of topo I could fully convert the supercoiled pBR322 DNA to fully relaxed topoisomers (Fig. 6(A), Lane 5). After the incubation of DNA with topo I, the appearance of the slowest moving bands of more relaxed DNA can be seen on the gel image (Fig. 6(A–E), Lane 5) The disappearance or the decrease in the intensity of the slowest moving band upon incubation of DNA, topo I and the complexes is the indication of topo I inhibition. The degree of inhibition of Topo I increases with increasing concentration (5–160 μM) of the complexes (Fig. 6(B–E)). But, the function of topo I is not fully inhibited even up to 160 μM of the complexes.

Among the compounds, compound **4** is slightly more active than the others because it started to inhibit topo I at 40 μM (Fig. 6(C), Lane 10). On the other hand, the least active compound **5**, shows no inhibition at 40 μM (Fig. 6(D), Lane 10). It is obvious that the addition of phen into the copper (II) hydrazone complex causes a lowering in the inhibitory concentration of topo I. By comparing the results of cytotoxicity and topo I inhibition assay for the ternary complexes, it seem likely that the cytotoxicities of the compounds are directly proportional to the topo I inhibition ability. Complex **4** with the lowest IC_{50} value of 3.2 μM appeared to be the most active topo I inhibitor (Fig. 6(C)). However, there is no direct correlation between the topo I inhibition activity of complex **3** (without N, N ligand) with its cytotoxicity. Of primary concern is the inevitable interaction between all the compounds with DNA without addition of topo I that would lead to the decline in rate of DNA migration (Fig. 6(A–E), Lane 3). To this end, it is logical to assume that the

Table 4
Hydrogen bonds for compounds **1, 2, 4** and **5**.

D-h···a	d (D-H) (Å)	d (H···A) (Å)	d (*D*···A) (Å)	<DHA (°)
Compound **1**				
O3–H3···Cl1	0.84	2.17	2.996 (2)	169.8
O1–H1···Cl2_#1	0.84	2.14	2.983 (2)	176.3
Symmetry operation#1: $-x, -y+1, -z$				
Compound **2**				
O3–H3A···N3	0.84	1.79	2.529	144.9
O1–H1···N1	0.84	1.84	2.576	145.5
O5–H5A···Cl2	1.04 (4)	2.07 (4)	3.105 (2)	178 (3)
O5–H5B···Cl1_#1	0.92 (4)	2.30 (4)	3.211 (2)	170 (3)
O6–H6A···Cl1_#1	0.88 (4)	2.45 (4)	3.276 (2)	158 (3)
O6–H6B···Cl2	0.78 (4)	2.40 (4)	3.178 (2)	172 (4)
N4–H4A···Cl1_#1	0.97 (3)	2.33 (3)	3.272 (2)	162 (2)
N2–H2A···Cl2	0.86 (3)	2.29 (3)	3.138 (2)	173 (3)
Symmetry operation#1: $x+1, y, z$				
Compound **4**				
O3–H3A···Cl1_#1	0.84	2.28	3.097 (2)	162.9
O4–H4A···O1	0.84	1.96	2.833	175.6
Symmetry operation#1: $x, y+1, z$				
Compound **5**				
O3–H3A···Cl1	0.71 (4)	2.51 (4)	3.219 (2)	179 (4)
O4–H4A···O1_#1	0.80 (4)	2.01 (4)	2.796	170 (4)
O3–H3B···Cl1_#2	0.74 (3)	2.50 (3)	3.243 (2)	178 (3)
O4–H4B···Cl1_#2	0.87 (4)	2.35 (4)	3.205 (2)	170 (3)
Symmetry operation#1: $-x+1, -y, -z+1$				
Symmetry operation#2: $-x+1, -y+1, -z$				

Table 5
The cytotoxicity activity for compounds **1-6** on A549, PC-3 and MRC-5 cells respectively.

Compounds	Cytotoxicity IC_{50} (μM)			
	A549	PC-3	MRC-5	Selectivity index (SI)
1	>30	>30	>30	NA
2	>30	14.4 ± 2.6	12.2 ± 0.6	0.85
3	>30	16.6 ± 3.1	>30	NA
4	4.2 ± 0.8	3.2 ± 0.2	5.1 ± 0.3	1.59
5	>30	8.1 ± 0.5	12.8 ± 1.5	1.58
6	6.7 ± 1.7	4.6 ± 0.5	4.9 ± 0.1	1.07

SI = IC_{50} of MRC-5/IC_{50} of PC-3.

cationic complexes bind to DNA at high concentration and cause the DNA to travel slower because of the formation of DNA and metal complex aggregate with higher molecular weight or the decrease in the negative charge of the DNA due to the binding with the cationic complexes [42,56–58]. Therefore, we could not determine the concentration of compounds that lead to full inhibition of topo I.

In an attempt to obtain more insight into the inhibition activity of the topo I in this work, we used three variations of mixing the DNA, topo I and compounds **2**–**6** (60 μM) respectively for topo I inhibition assay. It is possible to predict a generalized mechanism of action of topo I inhibition based on the three variations of mixing. When the three components are mixed simultaneously, there is slight inhibition of topo I as can seen by the presence of the fastest moving band with low intensity (Form I) which consists of supercoiled DNA and poorly relaxed DNA (Fig. 7, Lane 5). Similar band can be observed by incubating DNA and compound **4** before the addition of topo I (Fig. 7, Lane 6). Interestingly, when compound **4** is incubated with topo I before the addition of DNA (Fig. 7, Lane 7), the intensity of the fastest moving bands are the highest (Form I). However, the slowest moving band still remains with lower intensity (Form II). These observations suggest that the mechanism of action for topo I inhibition is based on two pathways, one involving the binding of complex to DNA and the other comprise the binding of complex to topoisomerase. In light of these results, we can deduce that binding of complex to topo I is a preferred inhibition pathway regardless of the structures of the complexes (Fig. 7, S3–S5 Lane 7). Nevertheless, continued research on this will hopefully lead to a better assessment of the usefulness of these compounds as anticancer drugs.

3. Conclusion

Mononuclear Cu(II) complexes of hydrazone ligand containing triphenylphosphonium moiety were synthesized and characterized. Their cell viability assay and topo I inhibition activity have been intensively studied. Crystal structure of **3** shows a distorted square planar geometry while **4** and **5** reveal similar distorted square pyramidal geometry. As previously mentioned, complex **4** gives rise to the lowest IC_{50} value against PC-3 cell lines. However, it can be seen that complex **5** has better selectivity among the compounds. In brief, DNA relaxation assay shows favourable results that all the compounds can inhibit topo I upon complexation and the binding through the enzyme seems to be the preferable inhibition pathway.

4. Experimental

4.1. Materials

Paraformaldehyde (BDH Limited poole Endland), salicyladehyde (Merck), triphenylphosphine (Merck), benzhydrazide (Sigma–Aldrich), 1,10′-phenanthroline (Acros), 2,2′-bipyridine, 5,5′-dimethyl-2,2′-bipyridine and copper(II) acetate monohydrate (Fluka) were used as received without further purification. All the solvents were of reagent grade. The pBR322, gene ruler 1 kb DNA ladder, 6× loading buffer and Tris-(hydroxymethyl)aminomethane (Tris) were procured from BioSyn Tech (Fermentas). Analytical grade agarose powder was obtained from Promega. Sodium chloride, human DNA topoisomerase I and ethidium bromide were purchased from Sigma Chemical Co. (USA). MTT (Methylthiazolyldiphenyl-tetrazolium bromide), RPMI 1640 medium, EMEM (Eagle's Minimum Essential Medium), sodium bicarbonate, *cis*-platin, carboxymethyl cellulose, EDTA, DMSO were purchased from Sigma–Aldrich company. Foetal bovine serum, penicillin/streptomycin (100×), amphotericin B (250 μg/mL) and sodium pyruvate (100 mM) were from PAA Laboratories.

4.2. Physical measurements

IR spectra were recorded as KBr pellets by using a Perkin–Elmer Spectrum RX-1 FTIR spectrophotometer. NMR spectra were recorded in deuterated DMSO-d_6 on a JEOL JNM GX-270 FT NMR System Spectrometer. Elemental analyses were performed on a Perkin–Elmer EA2400 CHNS elemental analyzer. UV–Vis spectroscopic measurements were carried out on a Perkin–Elmer Lambda 40 spectrophotometer.

4.3. Preparation of ligand and complexes

4.3.1. Synthesis of 5-(triphenylphosphoniummethyl)-salicylaldehyde (*1*)

The 5-chloromethylsalicylaldehyde was prepared according to the standard chloromethylation method by Huang and co-workers [59]. It was further reacted with triphenylphosphine to form a phosphonium salt by minor modification of the procedure reported by Wang and co-workers [60]. 5-chloromethylsalicylaldehyde (0.171 g, 1 mmol) and triphenylphosphine (0.262 g, 1 mmol) was refluxed in toluene (40 mL) for 5 h. The white solid formed was filtered, washed with toluene and air-dried. Crystals were formed by recrystallize using ethanol.

Yield: 78%, white solid, m.p.: 275–276 °C. Anal. Calc for $C_{26}H_{22}ClO_2P$: C, 72.14; H, 5.12. Found: C, 72.06; H, 5.15%. IR (KBr disc, cm^{-1}): $\nu_{(C=O)}$: 1676, $\nu_{(C-O)}$: 1112.

Characteristic: ^1H NMR (DMSO-d_6, TMS, ppm 400 MHz, s, singlet; d, doublet; t, triplet; m, multiplet): 11.10 (s, 1H, OH); 10.10 (s, 1H, CHO); 7.61–7.88 (m, 15H, aromatic CH); 6.91–7.18 (m, 3H, aromatic CH); 5.07–5.11 (d, J = 16 Hz, 2H, CH_2). ^{13}C NMR (DMSO-d_6, TMS, ppm 100 MHz): 189.41 (C=O); 160.83 (C–OH); 117.20–138.01 (Ar); 26.98, 27.44 (CH_2).

4.3.2. Synthesis of ligand [5-(triphenylphosphoniummethyl)-salicylaldehyde benzoylhydrazone] chloride monohydrate (*2*)

The ligand was synthesized by condensing benzhydrazide (0.136 g, 1 mmol) with compound **1** (0.433 g, 1 mmol) in ethanol (30 mL) for 4 h. Slow evaporation of the solvent yielded yellow crystals. The crystals were filtered, washed with cold ethanol and air-dried.

Yield: 85%, yellow solid, m.p.: 276–277 °C. Anal. Calc for $C_{33}H_{28}ClN_2O_2P\cdot H_2O$: C, 69.95; H, 5.31; N, 4.92. Found: C, 69.67; H, 5.41; N, 5.06%. IR (KBr disc, cm^{-1}): $\nu_{(C=O)}$: 1679, $\nu_{(C=N)}$: 1619, $\nu_{(N=N)}$: 1028.

Characteristic: ^1H NMR (DMSO-d_6, TMS, ppm 400 MHz, s, singlet; d, doublet; t, triplet; m, multiplet): 12.24 (s, 1H, NH); 11.39 (s, 1H, OH); 8.46 (s, 1H, CH=N); 7.91–7.93 (d, J = 8 Hz, 2H, aromatic CH); 7.86–7.89 (t, J = 7.2 Hz, 3H, aromatic CH); 7.63–7.72 (m, 12H, aromatic CH); 7.57–7.59 (d, J = 8 Hz, 1H, aromatic CH); 7.49–7.53 (t, J = 7.2 Hz, 2H, aromatic CH); 7.14 (s, 1H, aromatic CH); 6.76–6.83 (m, 2H, aromatic CH); 5.05–5.08 (d, J = 12 Hz, 2H, CH_2). ^{13}C NMR

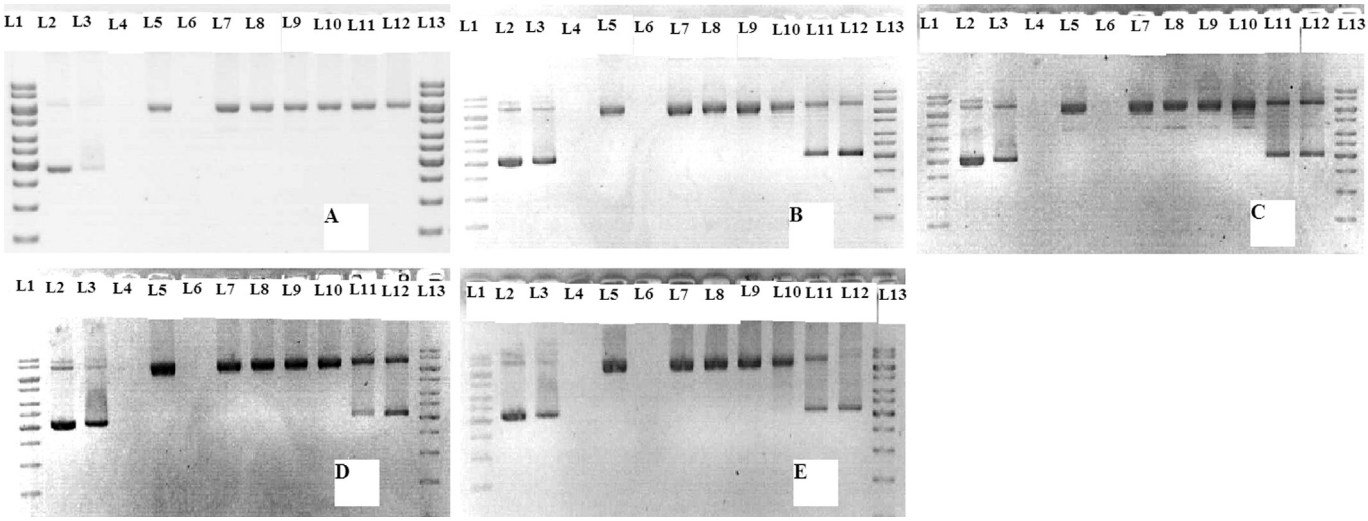

Fig. 6. Human topoisomerase I inhibition assay by gel electrophoresis. The gel images from **A**–**E** are for compounds **2**–**6**, respectively. Electrophoresis results of incubating human topoisomerase I (0.25 unit/20 μL) with pBR322 in the absence or presence of 5–160 μM of compound: Lane 1 and 13, gene ruler 1 Kb DNA ladder; Lane 2, DNA alone (control); Lane 3, DNA + 160 μM compound (control); Lane 5, DNA + 1 unit human topoisomerase I (control); Lane 7–12, DNA + 1 unit human topoisomerase I + varying concentration of compound; Lane 7, 5 μM; Lane 8, 10 μM; Lane 9, 20 μM; Lane 10, 40 μM; Lane 11, 80 μM; Lane 12, 160 μM.

(DMSO-d_6, TMS, ppm 100 MHz): 162.95 (C═O); 157.14 (C–OH); 146.80 (C═N); 116.82–135.12 (Ar); 27.09, 27.56 (CH_2).

4.3.3. Synthesis of chlorido[5-(triphenylphosphoniummethyl)-salicylaldehyde benzoylhydrazonato] copper(II) monohydrate (**3**)

Copper(II) acetate monohydrate (0.200 g, 1 mmol) and ligand (**2**) (0.551 g, 1 mmol) were refluxed in ethanol (30 mL) for 3 h. The green complex formed was filtered off and rinsed with cold ethanol. Crystals were formed by recrystallization using methanol.

Yield: 60%, green solid, m.p.: 244–245 °C. Anal. Calc for $C_{33}H_{27}ClCuN_2O_2P\cdot H_2O$: C, 62.86; H, 4.48; N, 4.44. Found: C, 63.37; H, 3.90; N, 4.58%. IR (KBr disc, cm^{-1}): $\nu_{(C=N)}$: 1613, $\nu_{(N=C)}$: 1503, $\nu_{(N=N)}$: 1047.

4.3.4. Synthesis of (1,10′-phenanthroline)[5-(triphenylphosphoniummethyl)-salicylaldehyde benzoylhydrazonato] copper(II) monohydrate ethanol (**4**)

Copper(II) acetate monohydrate (0.200 g, 1 mmol) and 1,10′-phenanthroline (0.180 g, 1 mmol) were heated in ethanol (20 mL) for 2 h followed by addition of ligand (**2**) (0.551 g, 1 mmol) in ethanol (20 mL) and the mixture was refluxed for another 2 h. The green complex formed was extracted with hexane and recrystallized from DMF-ethanol mixture.

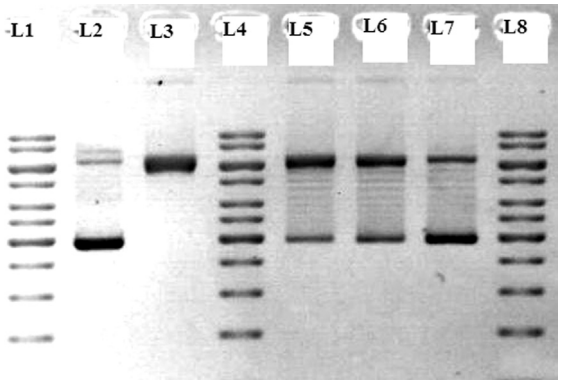

Fig. 7. Effect of sequence of mixing for the human topoisomerase I inhibition assay of complex **4**. Electrophoresis results of incubating human topoisomerase I (0.25 unit/20 μL) with pBR322: Lane 1, 4 and 8, gene ruler 1 Kb DNA ladder; Lane 2, DNA alone (control); Lane 3, DNA + 1 unit human topoisomerase I (control); Lane 5, DNA + 60 μM **4** + 1 unit human topoisomerase I, all components mixed at the same time; Lane 6, DNA + 60 μM **4** + 1 unit human topoisomerase I, DNA + complex **4** incubated for 30 min first before the addition of topo I; Lane 7, DNA + 60 μM **4** + 1 unit human topoisomerase I, complex **4** + topo I incubated for 30 min first before DNA is added.

Yield: 69%, green solid, m.p.: 178–180 °C. Anal. Calc for $C_{45}H_{36}ClCuN_4O_2P\cdot 2H_2O$ 1 EtOH: C, 64.38; H, 5.29; N, 6.39. Found: C, 63.84; H, 4.78; N, 6.11%. IR (KBr disc, cm^{-1}): $\nu_{(C=N)}$: 1612, $\nu_{(N=C)}$: 1501, $\nu_{(N=N)}$: 1046.

4.3.5. Synthesis of (2,2′-bipyridine)[5-(triphenylphosphoniummethyl)-salicylaldehyde benzoylhydrazonato] copper(II) dihydrate acetonitrile (**5**)

Same as complex **4** but using 2,2′-bipyridine instead of 1,10′-phenanthroline. The green complex formed was extracted with hexane and purified by recrystallization from acetonitrile-chloroform mixture.

Yield: 67%, green solid, m.p.: 108–110 °C. Anal. Calc for $C_{43}H_{36}ClCuN_4O_2P\cdot 3H_2O$: C, 62.62; H, 5.13; N, 6.79. Found: C, 63.02; H, 4.67; N, 6.30%. IR (KBr disc, cm^{-1}): $\nu_{(C=N)}$: 1612, $\nu_{(N=C)}$: 1502, $\nu_{(N=N)}$: 1043.

4.3.6. Synthesis of (5,5′-dimethyl-2,2′-bipyridine)[5-(triphenylphosphoniummethyl)-salicylaldehyde benzoylhydrazonato] copper(II) trihydrate (**6**)

Same as complex **4** but using 5,5′-dimethyl-2,2′-bipyridine instead of 1,10′-phenanthroline. The green powder formed was extracted with hexane and purified by methanol.

Yield: 71%, green solid, m.p.: 186–187 °C. Anal. Calc for $C_{43}H_{36}ClCuN_4O_2P\cdot 3H_2O$: C, 63.37; H, 5.44; N, 6.57. Found: C, 63.38; H, 5.10; N, 6.13%. IR (KBr disc, cm^{-1}): $\nu_{(C=N)}$: 1612, $\nu_{(N=C)}$: 1500, $\nu_{(N=N)}$: 1045.

4.4. X-ray crystallography

The unit cell parameters and the intensity data were collected on a Bruker SMART APEX CCD diffractometer, equipped with a Mo Kα X-ray source ($\lambda = 0.71073$ Å). The APEX2 software was used and the SAINT software for cell refinement and data reduction. Absorption corrections on the data were made using SADABS. The structures were solved and refined by SHELXL97 [61]. Molecular graphics were drawn by using XCEED [62]. The structures were

solved by direct-methods and refined by a full-matrix least-squares procedure on F^2 with anisotropic displacement parameters for non-hydrogen atoms.

4.5. Eschrichia coli topoisomerase I inhibition assay

The human DNA topoisomerase I inhibition activity was determined by measuring the relaxation of supercoiled plasmid DNA pBR322. For measurement of human topoisomerase I activity, the reaction mixtures were comprised of 10 mM Tris–HCl, pH 7.5, 100 nM NaCl, 1 mM phenylmethylsulfonyl fluoride, α-Toluenesulfonyl fluoride, PMSF, and 1 mM 2-mercatoethanol, 0.25 μg plasmid DNA pBR322, 1 unit of human topoisomerase I, and the test compound with final concentration of 160 μM. All reactions were conducted at a final volume of 20 μL and were prepared on ice. Upon enzyme addition, reaction mixtures were incubated at 37 °C for 30 min. The reactions were terminated by addition of 2 μL of 10% SDS, followed by 3 μL of dye solution comprising 0.02% bromophenol blue and 50% glycerol. SDS is required to observed a linear DNA fragment and to denature topoisomerase I, preventing further functional enzymatic activity. The mixtures were applied to 1.25% agarose gel and electrophoresed for 2 h at 80 V with running buffer of Tris-acetate EDTA (TAE) at pH 8.1. The gel was stained, destained, and photographed under UV light using a Syngene Bio Imaging system and the digital image was viewed with Gene Flash software.

In human topoisomerase I inhibition condition study, the same protocol was applied. This study is designed to deduce the mode of action of complexes in the human DNA topoisomerase I inhibition study. The sequence of addition of the main components (human DNA topoisomerase I, plasmid DNA pBR322, and metal complexes) was varied. For the first condition, human DNA topoisomerase I with the metal complex was incubated at 37 °C for 30 min before the addition of DNA. The mixture was incubated for another 30 min at the same temperature after the addition of DNA. As for the second condition, the metal complex and DNA was incubated for 30 min at 37 °C first, followed by the addition of topoisomerase I. This mixture was incubated for another 30 min at 37 °C after the addition of topoisomerase I.

4.6. Cell lines and culture medium

Human lung carcinoma (A549), human prostate adenocarcinoma (PC-3) and human non-cancer fibroblast (MRC-5) cell lines were purchased from American Type Culture Collection (ATCC, USA). A549 and PC-3 cells were maintained in RPMI 1640 medium while MRC-5 cells were maintained in EMEM medium, supplemented with 10% foetal bovine serum, 2% penicillin/streptomycin (100×) and 1% amphotericin B. The cells were cultured at 37 °C in humidified atmosphere in a CO_2 incubator (Shel Lab water-jacketed, USA).

4.7. MTT Cytotoxicity assay

The MTT cytotoxicity assay was carried out as previously described by Mosmann [63]. All samples were dissolved in DMSO to form stock solution before cytotoxicity testing. The final concentration of DMSO in each well was 0.5%. The cytotoxicity of each sample was expressed as IC_{50} value, which is the concentration of sample that reduced the viability of cells by 50% compared to the control (cells treated with 0.5% DMSO). All the samples were assayed in triplicate.

4.8. Statistical analysis

The IC_{50} values for cytotoxic activity were obtained by non-linear regression using GraphPad Prism statistical software.

Acknowledgement

We thank UM for financial support (RG148-11AFR). STC would like to thank UM for scholarship and financial assistance (PV089/2012A).

List of abbreviations

cisplatin	cis-diamminedichloroplatinum(II)
MTT	(3-(4,5-2-yl)-2,5-ditetrazolium bromide
DNA	DeoxyriboNucleic Acid
phen	1,10′-phenanthroline
bpy	2,2′-bipyridine
dbpy	5,5′-dimethyl-2,2′-bipyridine
DMSO	dimethylsulfoxide
DMF	dimethylformamide
Tris	tris-(hydroxymethyl)aminomethane
EMEM	Eagle's Minimum Essential Medium
EDTA	ethylenediaminetetraacetic acid
IR	infrared
KBr	potassium bromide
NMR	nuclear magnetic resonance
LMCT	ligand-to-metal-charge transfer
TAE	tris-acetate EDTA
SI	selectivity index

Appendix A. Supplementary data

Supplementary data related to this article can be found at http://dx.doi.org/10.1016/j.ejmech.2014.02.049.

References

[1] Y. Jung, S.J. Lippard, Direct cellular responses to platinum-induced DNA damage, Chemical Reviews 107 (2007) 1387–1407.
[2] X. Wang, Z. Guo, Towards the rational design of platinum(II) and gold(III) complexes as antitumour agents, Dalton Trans (2008) 1521–1532.
[3] M. Helena Garcia, T.S. Morais, P. Florindo, M.F.M. Piedade, V. Moreno, C. Ciudad, V. Noe, Inhibition of cancer cell growth by ruthenium(II) cyclopentadienyl derivative complexes with heteroaromatic ligands, Journal of Inorganic Biochemistry 103 (2009) 354–361.
[4] C.H. Wu, D.H. Wu, X. Liu, G. Guoyiqibayi, D.D. Guo, G. Lv, X.M. Wang, H. Yan, H. Jiang, Z.H. Lu, Ligand-based neutral ruthenium(II) arene complex: selective anticancer action, Inorganic Chemistry Communications 48 (2009) 2352–2354.
[5] C. Marzano, M. Pellei, F. Tisato, C. Santini, Copper complexes as anticancer agents, Anti-Cancer Agents in Medicinal Chemistry 9 (2009) 185–211.
[6] C. Marzano, M. Pellei, D. Colavito, S. Alidori, G.G. Lobbia, V. Gandin, F. Tisato, C. Santini, Synthesis, characterization, and in vitro antitumor properties of tris(hydroxymethyl)phosphine copper(I) complexes containing the new bis(1,2,4-triazol-1-yl)acetate ligand, Journal of Medicinal Chemistry 49 (2006) 7317–7324.
[7] E. García-Moreno, S. Gascón, M.J. Rodriguez-Yoldi, E. Cerrada, M. Laguna, S-Propargylthiopyridine phosphane derivatives as anticancer agents: characterization and antitumor activity, Organometallics 32 (2013) 3710–3720.
[8] F. Tisato, C. Marzano, M. Porchia, M. Pellei, C. Santini, Copper in diseases and treatments, and copper-based anticancer strategies, Medicinal Research Reviews 30 (2010) 708–749.
[9] A.W. Tai, E.J. Lien, M.M.C. Lai, T.A. Khwaja, Novel N-hydroxyguanidine derivatives as anticancer and antiviral agents, Journal of Medicinal Chemistry 27 (1984) 236–238.
[10] P.H. Wang, J.G. Keck, E.J. Lien, M.M.C. Lai, Design, synthesis, testing, and quantitative structure–activity relationship analysis of substituted salicylaldehyde Schiff bases of 1-amino-3-hydroxyguanidine tosylate as new antiviral agents against coronavirus, Journal of Medicinal Chemistry 33 (1990) 608–614.
[11] P. Krishnamoorthy, P. Sathyadevi, A.H. Cowley, R.R. Butorac, N. Dharmaraj, Evaluation of DNA binding, DNA cleavage, protein binding and in vitro

cytotoxic activities of bivalent transition metal hydrazone complexes, European Journal of Medicinal Chemistry 46 (2011) 3376–3387.
[12] G. Tamasi, L. Chiasserini, L. Savini, A. Sega, R. Cini, Structural study of ribonucleotide reductase inhibitor hydrazones. Synthesis and X-ray diffraction analysis of a copper(II)-benzoylpyridine-2-quinolinyl hydrazone complex, Journal of Inorganic Biochemistry 99 (2005) 1347–1359.
[13] C. Fan, H. Su, J. Zhao, B. Zhao, S. Zhang, J. Miao, A novel copper complex of salicylaldehyde pyrazole hydrazone induces apoptosis through up-regulating integrin β4 in H322 lung carcinoma cells, European Journal of Medicinal Chemistry 45 (2010) 1438–1446.
[14] Y. Zhang, L. Zhang, L. Liu, J. Guo, D. Wu, G. Xu, X. Wang, D. Jia, Anticancer activity, structure, and theoretical calculation of N-(1-phenyl-3-methyl-4-propyl-pyrazolone-5)-salicylidene hydrazone and its copper(II) complex, Inorganica Chimica Acta 363 (2010) 289–293.
[15] M. Alagesan, N.S.P. Bhuvanesh, N. Dharmaraj, Potentially cytotoxic new copper(ii) hydrazone complexes: synthesis, crystal structure and biological properties, Dalton Transactions 42 (2013) 7210–7223.
[16] D. Senthil Raja, N.S.P. Bhuvanesh, K. Natarajan, Synthesis, crystal structure and pharmacological evaluation of two new Cu(II) complexes of 2-oxo-1,2-dihydroquinoline-3-carbaldehyde (benzoyl) hydrazone: a comparative investigation, European Journal of Medicinal Chemistry 47 (2012) 73–85.
[17] D. Senthil Raja, E. Ramachandran, N.S.P. Bhuvanesh, K. Natarajan, Synthesis, structure and in vitro pharmacological evaluation of a novel 2-oxo-1,2-dihydroquinoline-3-carbaldehyde (2′-methylbenzoyl) hydrazone bridged copper(II) coordination polymer, European Journal of Medicinal Chemistry 64 (2013) 148–159.
[18] S. Banerjee, S. Mondal, S. Sen, S. Das, D.L. Hughes, C. Rizzoli, C. Desplanches, C. Mandal, S. Mitra, Four new dinuclear Cu(II) hydrazone complexes using various organic spacers: syntheses, crystal structures, DNA binding and cleavage studies and selective cell inhibitory effect towards leukemic and normal lymphocytes, Dalton Transactions (2009) 6849–6860.
[19] P.R. Reddy, A. Shilpa, N. Raju, P. Raghavaiah, Synthesis, structure, DNA binding and cleavage properties of ternary amino acid Schiff base-phen/bipy Cu(II) complexes, Journal of Inorganic Biochemistry 105 (2011) 1603–1612.
[20] S. Tabassum, A. Asim, F. Arjmand, M. Afzal, V. Bagchi, Synthesis and characterization of copper(II) and zinc(II)-based potential chemotherapeutic compounds: their biological evaluation viz. DNA binding profile, cleavage and antimicrobial activity, European Journal of Medicinal Chemistry 58 (2012) 308–316.
[21] N. Farrell, Biomedical uses and applications of inorganic chemistry. An overview, Coordination Chemistry Reviews 232 (2002) 1–4.
[22] M.X. Li, L.Z. Zhang, C.L. Chen, J.Y. Niu, B.S. Ji, Synthesis, crystal structures, and biological evaluation of Cu(II) and Zn(II) complexes of 2-benzoylpyridine Schiff bases derived from S-methyl- and S-phenyldithiocarbazates, Journal of Inorganic Biochemistry 106 (2012) 117–125.
[23] T.D. Pfister, W.C. Reinhold, K. Agama, S. Gupta, S.A. Khin, R.J. Kinders, R.E. Parchment, J.E. Tomaszewski, J.H. Doroshow, Y. Pommier, Topoisomerase I levels in the NCI-60 cancer cell line panel determined by validated ELISA and microarray analysis and correlation with indenoisoquinoline sensitivity, Molecular Cancer Therapeutics 8 (2009) 1878–1884.
[24] F. Zunino, G.L. Beretta, P. Perego, Targeting topoisomerase I: molecular mechanisms and cellular determinants of response to topoisomerase I inhibitors, Expert Opinion on Therapeutic Targets 12 (2008) 1243–1256.
[25] M.L. Rothenberg, Topoisomerase I inhibitors: review and update, Annals of Oncology 8 (1997) 837–855.
[26] K.W. Tan, H.L. Seng, F.S. Lim, S.-C. Cheah, C.H. Ng, K.S. Koo, M.R. Mustafa, S.W. Ng, M.J. Maah, Towards a selective cytotoxic agent for prostate cancer: interaction of zinc complexes of polyhydroxybenzaldehyde thiosemicarbazones with topoisomerase I, Polyhedron 38 (2012) 275–284.
[27] D.S. Pandey, S.K. Singh, S. Joshi, A.R. Singh, J.K. Saxena, DNA binding and topoisomerase II inhibitory activity of water-soluble ruthenium(II) and rhodium(III) complexes, Inorganic Chemistry 46 (2007) 10869–10876.
[28] S. Tabassum, W.M. Al-Asbahy, M. Afzal, F. Arjmand, V. Bagchi, Molecular drug design, synthesis and structure elucidation of a new specific target peptide based metallo drug for cancer chemotherapy as topoisomerase i inhibitor, Dalton Transactions 41 (2012) 4955–4964.
[29] P.B. Sreeja, M.R.P. Kurup, A. Kishore, C. Jasmin, Spectral characterization, X-ray structure and biological investigations of copper(II) ternary complexes of 2-hydroxyacetophenone 4-hydroxybenzoic acid hydrazone and heterocyclic bases, Polyhedron 23 (2004) 575–581.
[30] U.L. Kala, S. Suma, M.R.P. Kurup, S. Krishnan, R.P. John, Synthesis, spectral characterization and crystal structure of copper(II) complexes of 2-hydroxyacetophenone-N(4)-phenyl semicarbazone, Polyhedron 26 (2007) 1427–1435.
[31] M.R. Maurya, S. Khurana, C. Schulzke, D. Rehder, Dioxo- and oxovanadium(V) complexes of biomimetic hydrazone ONO donor ligands: synthesis, characterisation, and reactivity, European Journal of Medicinal Chemistry (2001) 779–788.
[32] T. Ghosh, S. Bhattacharya, A. Das, G. Mukherjee, M.G.B. Drew, Synthesis, structure and solution chemistry of mixed-ligand oxovanadium(IV) and oxovanadium(V) complexes incorporating tridentate ONO donor hydrazone ligands, Inorganica Chimica Acta 358 (2005) 989–996.
[33] P. Sathyadevi, P. Krishnamoorthy, M. Alagesan, K. Thanigaimani, P. Thomas Muthiah, N. Dharmaraj, Synthesis, crystal structure, electrochemistry and studies on protein binding, antioxidant and biocidal activities of Ni(II) and Co(II) hydrazone complexes, Polyhedron 31 (2012) 294–306.
[34] P. Talukder, A. Datta, S. Mitra, G. Rosair, M. Salah El Fallah, J. Ribas, End-to-end single cyanato and thiocyanato bridged Cu(II) polymers with a new tridentate Schiff base ligand: crystal structure and magnetic properties, Dalton Transactions (2004) 4161–4167.
[35] C. Rajarajeswari, R. Loganathan, M. Palaniandavar, E. Suresh, A. Riyasdeen, M.A. Akbarsha, Copper(II) complexes with 2NO and 3N donor ligands: synthesis, structures and chemical nuclease and anticancer activities, Dalton Transactions 42 (2013) 8347–8363.
[36] E.C. Constable, C.E. Housecroft, B.M. Kariuki, N. Kelly, C.B. Smith, How well do we understand self-assembly algorithms? From prototype grid to polymers, Comptes Rendus Chimie 5 (2002) 425–430.
[37] S. Roy, P. Mitra, A.K. Patra, Cu(II) complexes with square pyramidal (N 2S)CuCl 2 chromophore: Jahn-Teller distortion and subsequent effect on spectral and structural properties, Inorganica Chimica Acta 370 (2011) 247–253.
[38] A.W. Addison, T.N. Rao, J. Reedijk, J. Van Rijn, G.C. Verschoor, Synthesis, structure, and spectroscopic properties of copper(II) compounds containing nitrogen-sulphur donor ligands; the crystal and molecular structure of aqua [1,7-bis(N-methylbenzimidazol-2′;-yl)-2,6-dithiaheptane]copper(II) perchlorate, Journal of the Chemical Society, Dalton Transactions (1984) 1349–1356.
[39] P. Jaividhya, R. Dhivya, M.A. Akbarsha, M. Palaniandavar, Efficient DNA cleavage mediated by mononuclear mixed ligand copper(II) phenolate complexes: the role of co-ligand planarity on DNA binding and cleavage and anticancer activity, Journal of Inorganic Biochemistry 114 (2012) 94–105.
[40] I. Husain, J.L. Mohler, H.F. Seigler, J.M. Besterman, Elevation of topoisomerase I messenger RNA, protein, and catalytic activity in human tumors: demonstration of tumor-type specificity and implications for cancer chemotherapy, Cancer Research 54 (1994) 539–546.
[41] A.I. Tomaz, T. Jakusch, T.S. Morais, F. Marques, R.F.M. De Almeida, F. Mendes, É.A. Enyedy, I. Santos, J.C. Pessoa, T. Kiss, M.H. Garcia, [RuII(η5-C5H5(bipy)(PPh3)]+, a promising large spectrum antitumor agent: cytotoxic activity and interaction with human serum albumin, Journal of Inorganic Biochemistry 117 (2012) 261–269.
[42] M.S. Mohamed, A.A. Shoukry, A.G. Ali, Synthesis and structural characterization of ternary Cu (II) complexes of glycine with 2,2′-bipyridine and 2,2′-dipyridylamine. The DNA-binding studies and biological activity, Spectrochimica Acta, Part A 86 (2012) 562–570.
[43] C.-H. Ng, W.-S. Wang, K.-V. Chong, Y.-F. Win, K.-E. Neo, H.-B. Lee, S.-L. San, R.N.Z. Raja Abd. Rahman, W.K. Leong, Ternary copper(II)-polypyridyl enantiomers: aldol-type condensation, characterization, DNA-binding recognition, BSA-binding and anticancer property, Dalton Transactions 42 (2013) 10233–10243.
[44] T.S. Morais, F.C. Santos, T.F. Jorge, L. Côrte-Real, P.J.A. Madeira, F. Marques, M.P. Robalo, A. Matos, I. Santos, M.H. Garcia, New water-soluble ruthenium(II) cytotoxic complex: biological activity and cellular distribution, Journal of Inorganic Biochemistry 130 (2014) 1–14.
[45] T.S. Kamatchi, N. Chitrapriya, H. Lee, C.F. Fronczek, F.R. Fronczek, K. Natarajan, Ruthenium(II)/(III) complexes of 4-hydroxy-pyridine-2,6-dicarboxylic acid with PPh 3/AsPh 3 as co-ligand: impact of oxidation state and co-ligands on anticancer activity in vitro, Dalton Transactions 41 (2012) 2066–2077.
[46] P.J. Barnard, S.J. Berners-Price, Targeting the mitochondrial cell death pathway with gold compounds, Coordination Chemistry Reviews 251 (2007) 1889–1902.
[47] O. Rackham, S.J. Nichols, P.J. Leedman, S.J. Berners-Price, A. Filipovska, A gold(I) phosphine complex selectively induces apoptosis in breast cancer cells: implications for anticancer therapeutics targeted to mitochondria, Biochemical Pharmacology 74 (2007) 992–1002.
[48] T. Srdić-Rajić, M. Zec, T. Todorović, K. Anelković, S. Radulovi&cacute, Non-substituted N-heteroaromatic selenosemicarbazone metal complexes induce apoptosis in cancer cells via activation of mitochondrial pathway, European Journal of Medicinal Chemistry 46 (2011) 3734–3747.
[49] S. Sunami, T. Nishimura, I. Nishimura, S. Ito, H. Arakawa, M. Ohkubo, Synthesis and biological activities of topoisomerase I inhibitors, 6-arylmethylamino analogues of edotecarin, Journal of Medicinal Chemistry 52 (2009) 3225–3237.
[50] Y. Pommier, Topoisomerase I inhibitors: camptothecins and beyond, Nature Reviews Cancer 6 (2006) 789–802.
[51] B.A. Teicher, Next generation topoisomerase I inhibitors: rationale and biomarker strategies, Biochemical Pharmacology 75 (2008) 1262–1271.
[52] J.C. Wang, DNA topoisomerases, Annual Review of Biochemistry 65 (1996) 635–692.
[53] J.C. Wang, Cellular roles of DNA topoisomerases: a molecular perspective, Nature Reviews Molecular Cell Biology 3 (2002) 430–440.
[54] W. Feng, M. Satyanarayana, Y.C. Tsai, A.A. Liu, L.F. Liu, E.J. LaVoie, Novel topoisomerase I-targeting antitumor agents synthesized from the N, N,N-trimethylammonium derivative of ARC-111, 5H-2,3-dimethoxy-8,9-methylenedioxy-5-[(2-N, N,N-trimethylammonium)ethyl]dibenzo[c,h][1,6]naphthyridin-6-one iodide, European Journal of Medicinal Chemistry 44 (2009) 3433–3438.
[55] C. Marchand, S. Antony, K.W. Kohn, M. Cushman, A. Ioanoviciu, B.L. Staker, A.B. Burgin, L. Stewart, Y. Pommier, A novel norindenoisoquinoline structure reveals a common interfacial inhibitor paradigm for ternary trapping of the topoisomerase I-DNA covalent complex, Molecular Cancer Therapeutics 5 (2006) 287–295.

[56] R.L. Williams, H.N. Toft, B. Winkel, K.J. Brewer, Synthesis, characterization, and DNA binding properties of a series of Ru, Pt mixed-metal complexes, Inorganic Chemistry 42 (2003) 4394–4400.
[57] K.Y. Lee, I.C. Kwon, Y.H. Kim, W.H. Jo, S.Y. Jeong, Preparation of chitosan self-aggregates as a gene delivery system, Journal of Controlled Release 51 (1998) 213–220.
[58] J. Annaraj, S. Srinivasan, K.M. Ponvel, P.R. Athappan, Mixed ligand copper(II) complexes of phenanthroline/bipyridyl and curcumin diketimines as DNA intercalators and their electrochemical behavior under Nafion® and clay modified electrodes, Journal of Inorganic Biochemistry 99 (2005) 669–676.
[59] C. Huang, S. Gou, H. Zhu, W. Huang, Cleavage of C–S bonds with the formation of a tetranuclear Cu(I) cluster, Inorganic Chemistry 46 (2007) 5537–5543.
[60] J. Wang, C.T. Yang, Y.S. Kim, S.G. Sreerama, Q. Cao, Z.B. Li, Z. He, X. Chen, S. Liu, ^{64}Cu-labeled triphenylphosphonium and triphenylarsonium cations as highly tumor-selective imaging agents, Journal of Medicinal Chemistry 50 (2007) 5057–5069.
[61] G.M. Sheldrick, A short history of SHELX, Acta Crystallographica, Section A: Foundations of Crystallography 64 (2007) 112–122.
[62] L.J. Barbour, X-seed – a software tool for supramolecular crystallography, Journal of Supramolecular Chemistry 1 (2001) 189–191.
[63] T. Mosmann, Rapid colorimetric assay for cellular growth and survival: application to proliferation and cytotoxicity assays, Journal of Immunological Methods 65 (1983) 55–63.